PIC SIMULATIONS OF BEAM DYNAMICS EXPERIMENTS PLANNED FOR THE HIGH CURRENT EXPERIMENT[*]

C.M. Celata, Lawrence Berkeley National Laboratory, Berkeley, CA, U.S.A.
I. Haber, Naval Research Laboratory, Washington,D.C., U.S.A.
D.P. Grote, Lawrence Livermore National Laboratory, Livermore, CA, U.S.A.

Abstract

This paper reports progress on simulation of the High Current Experiment (HCX), a heavy ion accelerator at LBNL built to explore transport of intense beams at the scale of a heavy ion fusion power plant driver. The 2D particle-in-cell (PIC) code WARPxy was used to the explore the effect of image forces, distribution function, and focusing nonlinearities on the dynamic aperture of the electrostatic focusing system for the HCX, as well as the effect on dynamics of misalignments and quadrupole rotations. Simulations using a semigaussian initial distribution are compared to results for a more realistic distribution function obtained by initializing a space-charge-dominated beam at the emitter and propagating it through the aberrations of the injector and matching section.

1 INTRODUCTION

Phase 1 of the High Current Experiment (HCX) is presently being built by the Heavy Ion Fusion Virtual National Laboratory at Lawrence Berkeley National Laboratory. Phase 1 is a coasting-beam experiment which transports a beam of K^+ through 40 electrostatic quadrupoles, followed by four magnetic quadrupoles. Several important experiments are planned for the HCX, including measurements to determine the dynamic aperture of the electrostatic focusing system. The dynamic aperture has great significance for the cost of a heavy ion

Figure 1. HCX Electrostatic Quadrupole FODO Lattice

fusion driver, an induction linac which will accelerate many (~100) individually-focused beams in parallel to a target. The front end of this machine is expected to use electrostatic focusing. The cost of the induction cores encircling the focusing arrays is a major cost, and the diameter of these cores depends on the beam aperture needed. For the intense beams of interest, space charge is a major potential source of nonlinearity, and image forces are expected to be important to limitations on the aperture. Simulations of the dynamic aperture experiment using the 2D (transverse) version of the PIC code WARP [1] will be the main focus of this paper. We will also discuss simulations of misalignments of the beam, and quadrupole rotation errors. The HCX will have a rotatable quadrupole, which can be used to measure the effects of quadrupole rotation errors. Steering will also be possible, and can be used both to correct the alignment of the beam coming from the injector, and to intentionally introduce misalignments, in order to study their effects.

2 SIMULATION PARAMETERS

The HCX beam is presently envisioned to be a 700 mA, K^+ beam at 1.7 MeV, with the ratio of depressed to undepressed phase advance ~ 0.1. A portion of the FODO electrostatic lattice [2] is shown in Fig. 1. The radial distance from the center of the current channel to the quadrupole electrode surface is 2.30 cm, and the radius of the electrodes is set to 8/7 of this value in order to minimize the dodecapole nonlinearity of the focusing field. The effective length of the quadrupoles is 15.4 cm. For the simulations, the fields of the quadrupoles were first calculated using the 3D version of the WARP code, including the conducting electrodes and quadrupole end plates. At the z location of each timestep of the 2D simulation, the fields were decomposed into a set of multipole moments. The moments (up to $\cos(10\theta)$) were then used to construct the focusing forces on the particles for the 2D simulation. Thus the 2D simulations included fringe fields of the electrodes, nonlinearities of the field within the quadrupole, and image forces, which were calculated using the capacitive matrix technique.

The injector which will be used for the HCX has been in operation for some years and the beam has been heavily diagnosed, and simulated in 3D [3,4]. The main features of the beam, including a noticeable rim due to spherical aberration in the diode, are visible in the simulation. The beam passes from the diode to a section of the injector with electrostatic quadrupole focusing, where the azimuthal symmetry of the diode is broken. In this section
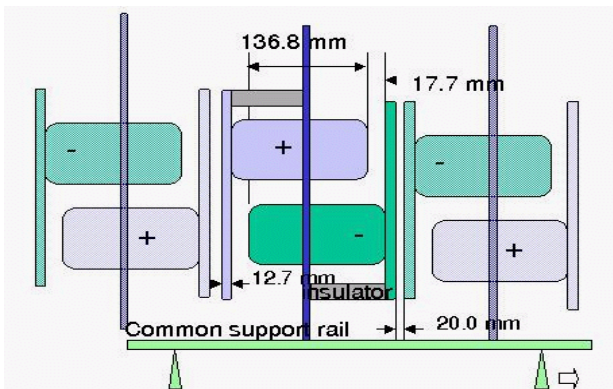
the rim breaks into separate peaks in the density distribution, which cause an ongoing density oscillation of particles into center of the beam and then out to the peaks. The nonuniform density of the beam can be decomposed into transverse collective modes of oscillation inherent in space-charge-dominated beams. Though the higher order modes will phase mix and interact, washing out quickly, the oscillation of the lowest order modes persists, giving the beam time-dependent peaks which are seen in the simulations.

The injector is followed by a matching section, which immediately precedes the HCX alternating gradient (AG) transport lattice. Aberrations in the matching section cause further distortions of phase space.

Two distribution functions were used as the initial distribution (initialized after the matching section) for the simulations in this paper. A semigaussian distribution (uniform in density, Maxwellian in velocity with uniform temperature given by the beam emittance), was used to study the dynamic aperture. Calculations were then done for comparison, using a distribution calculated by simulating from the emitter, using space-charge-limited injection, through the injector and matching section [4]. This self-consistent beam thus begins the simulation with the density oscillations and aberrations from the injector and matching system described above. Figure 2 shows the 2D spatial and phase space projections for this
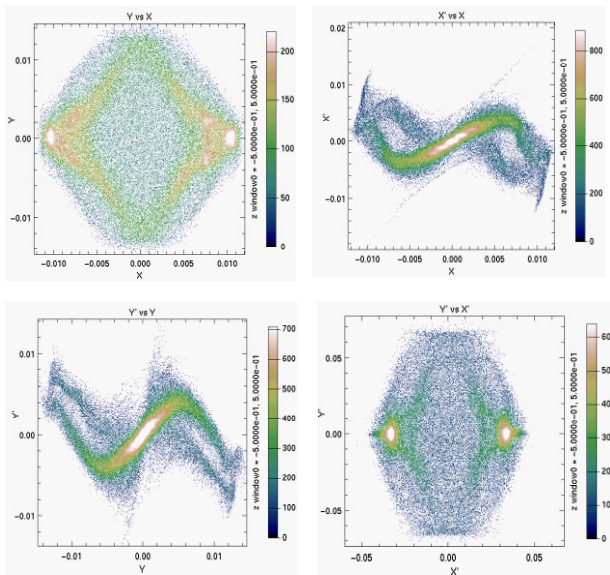

Fig. 2 Clockwise from top left: y vs. x, x' vs. x, y' vs. x', y' vs. y for the beam simulated from the emitter, shown at the entrance to the AG transport section of HCX.

initialization of the beam, which will be referred to below as the "more realistic" beam distribution, at the entrance to the AG lattice. The average xx' of the beam (where '=d/dz), which gives it a large slope in phase space, has been removed so that details of the distribution can be seen. The same has been done for yy'. It should be noted that the aberrations seen in these simulations have led to a probable change in HCX parameters-- it is likely that the

current will be decreased to 600 mA to decrease envelope size in the injector and matching section, decreasing nonlinearities sampled by the beam. The normalized emittance (normalized edge emittance, i.e., 4 x rms, will be used throughout this paper) chosen for the semigaussian was 0.63 π mm-mrad, which is four times the thermal emittance at the source (assuming 0.1 eV ion temperature), and close to the emittance of the more realistic distribution.

3 EFFECT OF NONLINEAR FOCUSING FIELDS AND IMAGE FORCES

We will discuss in this section primarily simulations done for an undepressed phase advance per lattice period of σ_0=60°. Simulations were done for σ_0 values from 45° to 80°, but 60° is the phase advance at which particle loss began (0.3% loss), so, as discussed below, this case can be considered as defining the dynamic aperture. At this focusing strength the maximum matched rms beam radius is 1.8-1.9 cm, depending on the distribution function, or about 80% of the quadrupole aperture. Simulations for the semigaussian were first done with only the quadrupole moment of the focusing fields included. The aperture was also increased to 2.4 times the initial beam radius at the center of a drift, in order to effectively eliminate image forces. The beam was matched to the transport lattice using an envelope code which included only the quadrupole moment (as a function of z) of the 3D field decomposition. This produced a nearly negligible mismatch in rms radius of +/− 0.5%. The rms emittance was essentially constant– it decreased slightly (~1%) during transport through 50 lattice periods, an effect well known for intense beams as the semigaussian relaxes.

Image forces were then added by placing the grounded conducting boundaries of the circular quadrupole electrodes at the proper location. Inclusion of images caused the mismatch to increase to +/− 3%. The beam shape began to oscillate, assuming a diamond shape at some z locations, as the edges of the beam were pulled toward the electrodes. Rms emittance in the x dimension increased initially by 0.1 π mm-mrad and then stayed constant. This level of increase is marginally measurable with present diagnostics, and is not significant for a driver.

When moments beyond the quadrupole were added, mismatch stayed about the same, showing that the effect of images dominates the effect of focusing nonlinearities in the mismatch. Emittance growth was also very similar to the previous case with image forces only– it is negligible– though with extra structure (peaks in emittance vs. z) at the z location of the fringe fields. The visible effects of transport on the beam were the growth of a small (~few mm) halo, and a few millimeter increase in the radius of the beam due to image forces.

As the value of σ_0 was decreased from 60° to 45°, increasing the size of the beam, the particle loss increased from 0.3% to 2% at 55°, 13% at 50°, and 24% at 45°.

Since fields at the edge of the aperture are not adequately modeled in this moment approximation, the exact amount of particle loss is probably not accurate. But it is notable that rms emittance growth remained negligible, showing that halo particles were quickly lost, with their large rms emittance contribution. In sum, the dynamic aperture seems to be evinced by particle loss, which occurs before any significant emittance changes. In reality, but not represented in the simulation, loss of heavy ions will produce electrons, neutrals, and ions which will interfere with beam propagation. Thus the particle loss we see in the calculations is likely to indeed be the aperture-limiting effect. We note that the particle loss is a gradual function of σ_0.

4 DISTRIBUTION FUNCTION EFFECTS

Transport of the more realistic beam distribution described above through 50 lattice periods was also simulated, again for the $\sigma_0=60°$ case, to explore the effect on the HCX experiments of the upstream beam aberrations. Beam loss and mismatch were very similar for the semigaussian and the more realistic beam. There was a slight (≈ 0.2 π mm-mrad) increase in the normalized emittance in one plane. The final phase spaces for the two beams are quite different, demonstrating that, as expected, the effects of the initial distribution function persist. The x-x' phase spaces for the two cases are shown in Fig. 3. As in Fig. 2, the average xx' of the beam has been removed. From this figure one can see that the more realistic beam has a lower temperature core, with more of the beam in halo. The halo in configuration space is approximately twice the width found for the semigaussian. For the case of $\sigma_0=80°$ with the more realistic beam, the halo is larger still, (≈ 5 mm), though the beam radius is much smaller (maximum matched radius is 1.6 cm). Thus the halo seems to be caused by mismatch and density oscillations, rather than to any aperture-limiting effect. Both semigaussian and more realistic beams have shapes that oscillate from diamond to elliptical due to image forces. Much more simulation is needed to confirm and explain what is seen here, but it appears that the HCX will be able to study halo formation from mismatch and density oscillations, and that the real beam could have similar particle loss aperture limitations to the idealized semigaussian.

5 QUADRUPOLE MISALIGNMENT AND ROTATION ERRORS

Simulations were also performed with a semigaussian initial distribution for beams initialized at the center of a drift with centroid angles of 6 and 12 milliradian, modelling misalignments. We describe here runs for $\sigma_0=60°$ with initial centroid velocity in the x direction. The beam centroid reached a maximum distance from the channel center of 4 and 7 mm respectively for the 6 and 12 mrad cases. The emittance change was negligible for

both, but changes in the phase space were evident and should be measurable. The beam edge toward the electrode was slightly pointed due to images. Particle loss was 1% and 15% respectively, after 20 lattice periods.

Rotations of the first quadrupole, which can be rotated in the experiment, were also studied briefly. A rotation of 4 degrees can be seen in the rotation of the diamond-shaped shape of the beam downstream, with attendant rotation in phase space. There was a 0.7 π mm-mrad increase in the generalized emittance, ε_g [5].
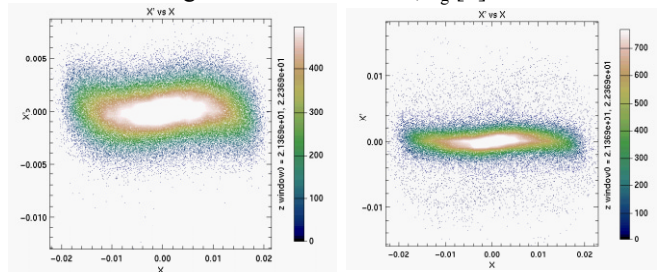

Figure 3. x-x' phase space for the semigaussian (left) and more realistic distribution function. z=21.8 m Vertical scales: −0.013 to 0.0085 (left), −0.018 to 0.018 (right).

6 SUMMARY

2D PIC simulations indicate that the signature of the dynamic aperture limit in the HCX is particle loss, rather than detectable changes in rms emittance. Halo formation through mismatch and density oscillation appears to be measurable. Misalignment or rotation of the quadrupoles causes changes in beam shape and orientation, but again, changes in rms emittance due to these mechanisms appear undetectable, at least in the length of the HCX electrostatic lattice.

7 REFERENCES

[1] David P. Grote, A. Friedman, I. Haber, W. Fawley, J. L. Vay, ``New Developments in WARP3d: Progress Toward End-to-End Simulation'', Nuclear Inst. and Methods in Physics Research, A, 415, Nos 1, 2, p 428, 1998.

[2] V. Karpenko et al., "An Engineering Overview of an Electrostatic Quadrupole Lattice for a High Current Transport Experiment", these proceedings.

[3] F. M. Bieniosek†, E. Henestroza, J. W. Kwan, L. Prost, P. Seidl, "2-Mv Injector For Hcx", these proceedings.

[4] E. Henestroza, F. Bieniosek, J. Kwan, A. Friedman, D. Grote, "Beam Dynamics Studies of the Injector and Matching Section for HCX", these proceedings.

[5] R. A. Kishek et al., "Effects of Quadrupole Rotations on the Transport of Space-Charge-Dominated Beams" Proc. of the Particle Accelerator Conference, March - 2 April, 1999, New York, NY, 1761.